FULL PAPER

Single-Photon Delay

ADVANCED
QUANTUM
TECHNOLOGIES
www.advquantumtech.com

Cesium-Vapor-Based Delay of Single Photons Emitted by Deterministically Fabricated Quantum Dot Microlenses

Lucas Bremer, Sarah Fischbach, Suk-In Park, Sven Rodt, Jin-Dong Song, Tobias Heindel, and Stephan Reitzenstein*

Quantum light sources are key building blocks of photonic quantum technologies. For many applications, it is of interest to control the arrival time of single photons emitted by such quantum devices, or even to store single photons in quantum memories. In situ electron beam lithography is applied to realize InGaAs quantum dot (QD)-based single-photon sources, which are interfaced with cesium (Cs) vapor to control the time delay of emitted photons. Via numerical simulations of the light–matter interaction in realistic QD-Cs-vapor configurations, the influence of the vapor temperature and spectral QD-atom detuning is explored to maximize the achievable delay in experimental studies. As a result, this hybrid quantum system allows to trigger the emission of single photons with a linewidth as low as 1.54 GHz even under non-resonant optical excitation and to delay the emission pulses by up to (15.71 ± 0.01) ns for an effective cell length of 150 mm. This work can pave the way for scalable quantum systems relying on a well-controlled delay of single photons on a time scale of up to a few tens of nanoseconds.

1. Introduction

Light–matter interaction in atomic vapors is a very attractive resource for applications in future quantum communication technologies.[1,2] It is particularly interesting for the realization of quantum memories with long storage times.[3,4] In addition, it can be used to frequency-lock single-photon sources with sub-GHz accuracy in large-scale quantum networks relying on entanglement swapping between different sources with identical emission wavelengths.[5] Controlling the propagation of single

L. Bremer, Dr. S. Fischbach, Dr. S. Rodt, Dr. T. Heindel,
Prof. S. Reitzenstein
Institute of Solid State Physics
Technische Universität Berlin
10623 Berlin, Germany
E-mail: stephan.reitzenstein@physik.tu-berlin.de
S.-I. Park, Dr. J.-D. Song
Center for Opto-Electronic Materials and Devices
Korea Institute of Science and Technology
Seoul 02792, Republic of Korea

The ORCID identification number(s) for the author(s) of this article can be found under https://doi.org/10.1002/qute.201900071

photons and the storage of quantum information are highly relevant to facilitate, for instance, the development of powerful quantum computers in the near future.[6] Moreover, to build large-scale quantum networks based on quantum repeater protocols,[1,7,8] network nodes are necessary to locally store the information encoded on single photons acting as flying qubits.[8,9] In this context, the generation of slow light by means of light–matter interaction in an atomic ensemble of alkali atoms has been known for several decades.[10] Only recently, advances in the development of quantum light sources have made it possible to combine the underlying physical principles and device functionalities in the form of hybrid quantum systems. Nowadays, self-assembled semiconductor quantum dots (QDs) allow one to realize close-to-ideal triggered sources of single and indistinguishable photons.[11–13]

Furthermore, advanced semiconductor nanotechnology platforms facilitate the deterministic integration of pre-selected QDs into photonic components with precisely engineered optical properties for instance in terms of the photon extraction efficiency.[12–14] Even the integration of alkali gases in photonic microstructures on a chip has been demonstrated in the past.[15] However, interfacing QDs with atomic vapors to form hybrid quantum systems with enhanced functionality, such as single-photon delay and photon storage, is highly challenging due to the intrinsic bandwidth mismatch between the two components and because of the precise spectral matching required to enable pronounced and reproducible light–matter interaction. While initial steps in this direction have already been taken,[4,16] storing individual quantum states in dilute vapors of alkali metals has not been mastered yet. Therefore, in order to establish the necessary technology and experimental techniques and to explore the underlying physics, it is useful to investigate single-photon time delay in a more accessible setting, namely by interaction with transitions in cesium (Cs) atoms with large dispersion.[17–19]

In our work, we aim at well-controlled light delay in a hybrid solid-state atom system based on a deterministically fabricated QD single-photon source (SPS). Deterministic process flows are undoubtedly of utmost importance when considering the future transfer of quantum technological concepts into large-scale practical applications, which require many precisely engineered and fabricated quantum devices. For this purpose, we

**ADVANCED
SCIENCE NEWS**

www.advancedsciencenews.com

**ADVANCED
QUANTUM
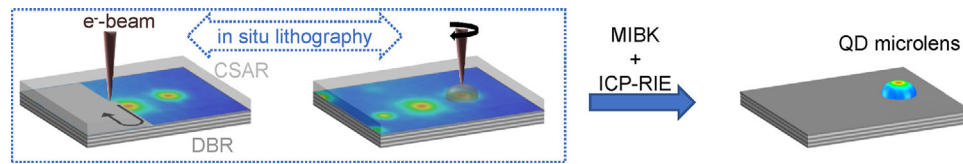TECHNOLOGIES**

www.advquantumtech.com

Figure 1. Schematic view presenting the deterministic fabrication of QD-microlenses by means of 3D in situ EBL: (From left to right) First, the sample, coated with an electron-sensitive resist (CSAR), is mapped at 10 K at a low electron dose of 2.5 mC cm^{-2} and the spatially and spectrally resolved cathodoluminescence signal is detected by a high-resolution grating spectrometer. In the following 3D in situ EBL process step, a lenticular dose profile is introduced into the resist at a higher dose of up to 17 mC cm^{-2} over selected QDs with suitable emission wavelength and emission intensity. Here, the electron dose is chosen to invert the resist locally, that is, to make it insoluble at the QD position. Afterward, the soluble resist is removed in the cleanroom using the developer methylisobutylketone (MIBK), so that the remaining resist (forming a microlens) above selected QDs acts as etch mask. In this way, the lens-profile can be transferred into the semiconductor material by the final inductively coupled plasma reactive-ion etching (ICP-RIE) step.

apply 3D in situ electron beam lithography (EBL) to pre-select and integrate bright InGaAs QDs with Cs-D$_1$ compatible wavelengths into microlenses with enhanced photon extraction efficiency. Numerical simulations are applied to determine optimum experimental and operation parameters for interfacing a QD SPS with dilute Cs vapor in a cell with variable temperature. Selecting the most suitable QD-atom detuning in the spectral range of minimum absorption in between the hyperfine-split components of the Cs-D$_1$ line we achieve complete normalized delays of up to (1.05 ± 0.01) ns cm^{-1}, which translates to an absolute delay of (15.71 ± 0.01) ns for a cell with an optical path length in Cs vapor of 150 mm and a temperature of 132.5 °C.

2. Sample Technology

The goal to interface QDs and atomic vapors with dissimilar optical properties, for instance in terms of transition linewidths, sets stringent demands on the quality and emission features of the solid-state-based single-photon emitters. First, the spectral detuning between the emission from the quantum emitter and the transitions of the atomic ensemble needs to be controlled precisely with sub-GHz accuracy. Secondly, spectrally narrow emission lines on a scale of GHz are required to ensure a complete pulse delay,[18,19] as we discuss below in more detail. Therefore, we designed and epitaxially grew a semiconductor heterostructure that includes a single layer of self-assembled InGaAs QDs as active medium. The wavelength of the QD ensemble emission band is centered at approximately 914 nm with a full-width at half-maximum (FWHM) of 30 nm. The heterostructure includes an AlGaAs/GaAs distributed Bragg reflector (DBR) consisting of 23 mirror pairs followed by a 63 nm GaAs buffer layer, the InGaAs QD layer with an areal density of ≈20 μm^{-2}, and a GaAs capping layer with a thickness of 400 nm.

The 400 nm thick GaAs capping layer allows us to realize monolithic GaAs microlenses on top of pre-selected QDs by means of in situ EBL, as we describe in the following. The microlenses, together with the lower DBR mirror, enhance the photon extraction efficiency of the embedded QDs from less than 1% for a simple planar structure to about 30% for an NA of 0.4.[12,20] The associated (broadband) enhancement of emission increases the single-photon flux and is thus very helpful for the envisaged QD-atom coupling experiments. Here, emission enhancement is of particular importance at elevated temperatures of the Cs vapor

where high single-photon delays can be achieved at the cost of increased optical absorption.

The deterministic QD-microlens fabrication is based on the powerful 3D in situ EBL technique,[21] as described in **Figure 1**. It uses a scanning electron microscope equipped with a helium (He) flow cryostat, an elliptical mirror, and a high-resolution spectrometer to perform cathodoluminescence (CL) spectroscopy at 10 K. Additionally, it includes a pattern generator with an extended home-built software kit allowing for joint operation and synchronization between CL spectroscopy and EBL. Based on this customized system, the deterministic fabrication process starts with CL mapping of about 50 μm × 50 μm write fields of the above-described QD-sample to identify suitable QDs based on their emission intensity and wavelength, which are required to match the target transitions of the Cs vapor near the D$_1$ line at 894.59296 nm in vacuum.[22] Prior to the in situ EBL process, the sample is spin-coated with an 85 nm thick layer of CSAR resist, which is exposed homogenously during the CL mapping by an electron beam dose of 2.5 mC cm^{-2}. Directly after CL mapping, the EBL software automatically selects suitable QDs within the target wavelength of (894.6 ± 0.5) nm. The electron beam is directed to the respective QD positions, where microlenses with a numerically optimized base width of 2.8 μm are written in the resist by varying the dose from 17.0 mC cm^{-2} at the center of the microlens to 4.5 mC cm^{-2} at its edge. In this way, the resist gets locally inverted so that it becomes insoluble in the subsequent development process which is performed at room temperature in the cleanroom after sample transfer. The resulting microlenses of resist material are aligned to the preselected QDs (about 3–5 QDs per write field) with 30–40 nm accuracy[23] and act as etch masks in the final plasma enhanced reactive ion etching step. In this highly anisotropic etching process, the uncovered semiconductor material is removed (including the QD layer in the write fields). The EBL written lens profile is transferred into the semiconductor material so that we obtain GaAs microlenses, each with single monolithically integrated pre-selected QDs with a process yield exceeding 90%. The resulting QD-based single-photon sources are well suited to explore the QD-atom interaction and temporal delay in Cs vapor as we experimentally show in Section 3.2.

3. Interfacing Single Photons with Atomic Vapor

To understand the influence of dense Cs vapor on the optical properties of a propagating light pulse, it is necessary to describe
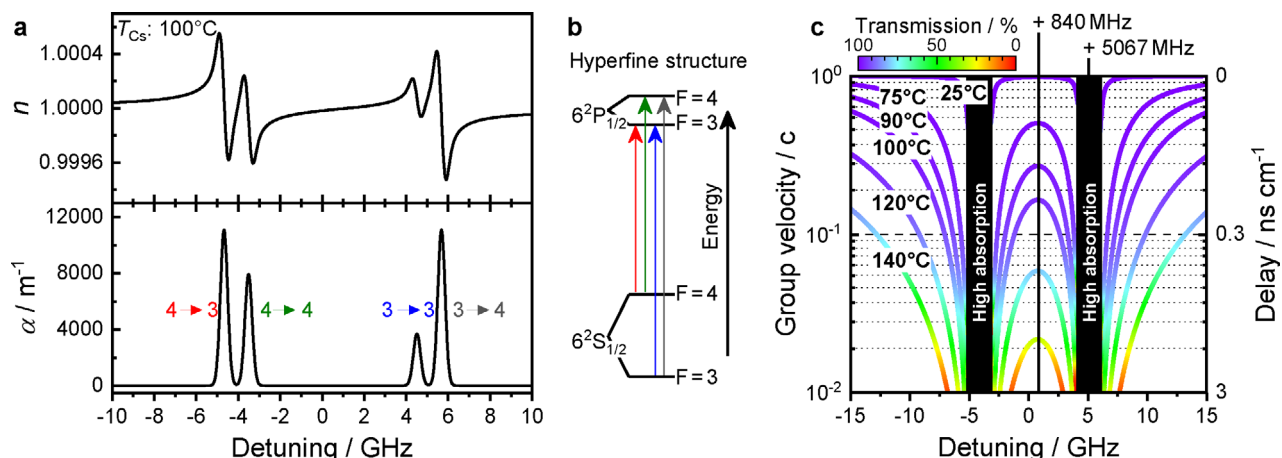
**ADVANCED
SCIENCE NEWS**
www.advancedsciencenews.com

**ADVANCED
QUANTUM
TECHNOLOGIES**
www.advquantumtech.com

Figure 2. a) The real part of the refractive index n and absorption coefficient α of Cs in the vicinity of the resonant frequency of the D_1 transition at a vapor temperature of 100 °C. While n (upper panel) shows the typical dispersion line shape, α (lower panel) is an inhomogeneously broadened Lorentz line for each of the four transitions between the four hyperfine energy levels. The curves are calculated with ElecSus.[24] b) Schematic presentation of the associated Cs-D_1 energy-level diagram with the hyperfine structure. c) Group velocity and the resulting temporal delay as a function of the spectral detuning from the Cs-D_1 line for various temperatures between 25 and 140 °C. The transmission of a 150 mm long Cs cell is color-coded as indicated by the scale bar.

the macroscopic response of matter to an incident electromagnetic wave. In the case of an optically thin non-polar gas, this description can be done by considering its electrical susceptibility. The susceptibility of the gas is strongly frequency dependent in the region of the intra-atomic transitions, which is discussed in Section 3.1. In Section 3.2, we perform numerical simulations to study wavelength dependent light–matter interaction effects in a diluted gas of Cs atoms. Subsequently, the theoretical results are compared to an experimentally observed controllable delay of light pulses from a QD-microlens.

3.1. Electric Susceptibility

The high interest in alkali atoms, and vapors thereof, in quantum nanophotonics is explained by their well-defined and comparatively simple energy-level scheme. This simplifies the theoretical description of the associated light–matter interaction and is beneficial for well-controlled experiments to explore and utilize this interaction. In fact, of all multi-electron atoms, alkaline elements are most similar to hydrogen, resulting in a simple energy-band diagram with distinct spectrally separated absorption lines.

Concerning the present experiment, only transitions within the non-degenerated energy level $6s^1$ of Cs are of relevance. The optical response of a dilute thermal vapor of Cs atoms to a propagating electromagnetic wave is given by its complex refractive index n_c, which can be derived in a textbook like manner from the weak-probe electric susceptibility χ given by

$$n_c = \sqrt{1 + \chi} \tag{1}$$

The electric susceptibility of an ensemble of Cs atoms is then calculated numerically using ElecSus,[24] which considers

temperature dependent Doppler- and self-broadening. The susceptibility is directly proportional to the number density of Cs atoms, which increases almost exponentially with temperature. **Figure 2**a shows an example of the real part of the refractive index n and the absorption coefficient α of Cs vapor for a temperature of 100 °C. The refractive index is approximately one for strong detuning from the D_1 resonance frequency and shows the typical dispersion line-shape associated with anomalous dispersion for all four transitions of the hyperfine structure (see Figure 2b). Based on the refractive index, it is possible to calculate the group velocity v_g via

$$v_g = \frac{c}{n}\left(1 - \frac{\omega}{n}\frac{dn}{d\omega}\right) \approx \frac{c}{n + \omega \, dn/d\omega} \tag{2}$$

where c is the speed of light and ω the angular frequency.[25] Considering Equation (2), it is obvious that in areas where the refractive index has a large positive gradient, a low group velocity—and thus a large delay—is to be expected as desired for many target applications in photonic quantum technology. Figure 2c shows the corresponding group velocity for various temperatures. The smallest group velocities are expected in the immediate vicinity of the resonance frequencies of the hyperfine structure. However, even at moderate temperatures the absorption in these regions is very high, and in practice, it is usually important to find a good balance between the lowest possible group velocity and the lowest possible optical absorption. For this purpose, it is important to know about the interdependence of delay, absorption, and vapor temperature, and **Figure 3** can serve as a decision-making aid. In Figure 3, the local maxima in the transmission of Cs vapor, resulting from the hyperfine splitting of the ground state (+840 MHz related to the Cs-D_1 line) and from the splitting of the excited state (+5067 MHz), are compared in relation to absorption and delay for different color-coded temperatures. The mirrored position at −4085 MHz is not shown for the sake of clarity, as the
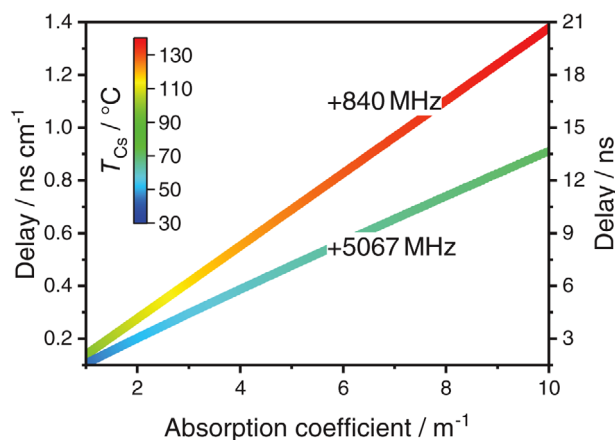
1900071 (3 of 8)

**ADVANCED
SCIENCE NEWS**

www.advancedsciencenews.com

**ADVANCED
QUANTUM
TECHNOLOGIES**

www.advquantumtech.com

Figure 3. Calculated delay as a function of the absorption coefficient for the spectral positions +840 and +5067 MHz relative to the Cs-D_1 line. The y-axis on the right side shows the resulting delay for a 150 mm long path through the Cs vapor corresponding to our experimental conditions. The corresponding Cs vapor temperature (T_{Cs}) is color-coded.

Figure 4. Schematic view of the spectroscopy setup used for micro-photoluminescence studies at cryogenic temperatures. The QD sample to be examined is placed in a He flow cryostat at a fixed temperature between 5 and 30 K. It is excited by a pulsed titanium–sapphire laser with a pulse length of 1.2 ps at a repetition rate of 80 MHz. After passing through optical elements of the detection path, light emitted by the QD is focused on the entrance slit of a monochromator, which decomposes the sample signal into its spectral components. The spectral information can be analyzed either with a CCD or are forwarded after spectral filtering to a fiber-coupled SPCM for time-resolved experiments or a high-resolution FPI. The additional CCD camera provides a white-light image to facilitate the adjustment and orientation on the sample surface.

curve is almost identical to the one for +5067 MHz. The position of −4085 MHz is therefore not discussed further in the following. The figure shows that for a given absorption coefficient, the delay time in case of +840 MHz detuning is always higher. For technical reasons (related to the maximum cell temperature of 120 °C), it is interesting to consider the spectral position at +5067 MHz for the QD–atom interaction, because it features larger delays than for +840 MHz detuning at low and intermediate temperatures. However, the higher dispersion of the group velocity must be considered for +5067 MHz detuning, which distorts light pulses of finite spectral width.

3.2. Delaying Single Photons

To experimentally explore the predicted temporal delay induced by light–matter interaction in Cs vapor, we used the spectroscopy setup depicted schematically in **Figure 4**. The excitation source is a pulsed titanium–sapphire laser operating in ps mode with a tunable emission wavelength between 700 and 1050 nm and a repetition frequency of 80 MHz. The sample is placed in a He flow cryostat at 11.8 K. In order to localize the structures to be investigated on the sample surface, the broadband light of a white light source is coupled into the beam path. The microscope objective used has a numerical aperture of 0.4 at 20 × magnification. A commercial Cs vapor cell with a length of 75 mm is used to delay single photons by controlled atom interaction in the Cs vapor. The cell was passed through twice to double the achievable delay by a total effective length of 150 mm. The temperature is controlled either by a negative temperature coefficient resistor located inside the housing of the vapor cell or more precisely by measuring the transmission of the Cs vapor using a tunable narrow-band CW laser. From the transmission, the temperature can be determined by a fit using ElecSus.[24] This method is much more accurate than the resistance measurement because it delivers the temperature of the Cs vapor itself. Using a grating
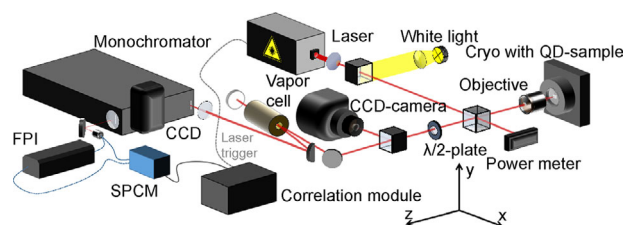
spectrometer equipped with a liquid-nitrogen-cooled Si charge-coupled device (CCD) camera with an overall spectral resolution of 25 µeV, emission of the QD line under study is spectrally analyzed and selected to match the wavelength of the target Cs transitions. Additionally, the setup includes a high-resolution confocal Fabry–Pérot interferometer (FPI) with a free spectral range of 7.5 GHz and a resolution of 0.43 µeV. For time-resolved µPL experiments the QD emission is directed via the lateral output slit of the monochromator to a Si avalanche photodiode based single photon counting module (SPCM) with a temporal resolution of 350 ps. The counting electronics of the correlation module allows us to measure the time difference between the trigger signal of the laser and the detection time of the SPCM for each detection event. The actual pulse delay due to the hot Cs vapor is obtained by relating the measured time interval to a reference measurement without a cell.

In our delay experiment, we used a QD integrated deterministically into a microlens as described in Section 2. **Figure 5** presents basic spectroscopic information about the investigated QD-microlens. Panel 5a shows a µPL spectrum of the QD line, which can be tuned into resonance with the Cs-D_1 line via temperature variation. The excitonic line of the investigated QD-microlens has an inhomogeneous linewidth of (1.54 ± 0.05) GHz (FWHM), as measured by the FPI (see Figure 5b) under pulsed off-resonant excitation at 800 nm. Noteworthy, the measured linewidth is by a factor of 7 larger than the homogenous linewidth of (0.22 ± 0.01) GHz estimated from time resolved measurements shown in Figure 5c. Here, the enhanced linewidth is attributed mainly to spectral diffusion due to excess carriers in the non-resonantly pumped QD system. Interestingly, the observed linewidth <3.0 GHz is even smaller compared to values observed under strict resonant excitation in ref. [19]. This highlights the high optical quality of our QD-microlenses. Figure 5d shows the second-order autocorrelation function $g^{(2)}(\tau)$ recorded with a fiber-coupled Hanbury Brown and Twiss (HBT)-type setup. The suppression of the multiphoton emission with $g^{(2)}(0) \ll 0.5$ clearly proofs single-photon emission.

In order to phenomenologically describe the influence of the Cs vapor on the single-photon pulse shape in the delay
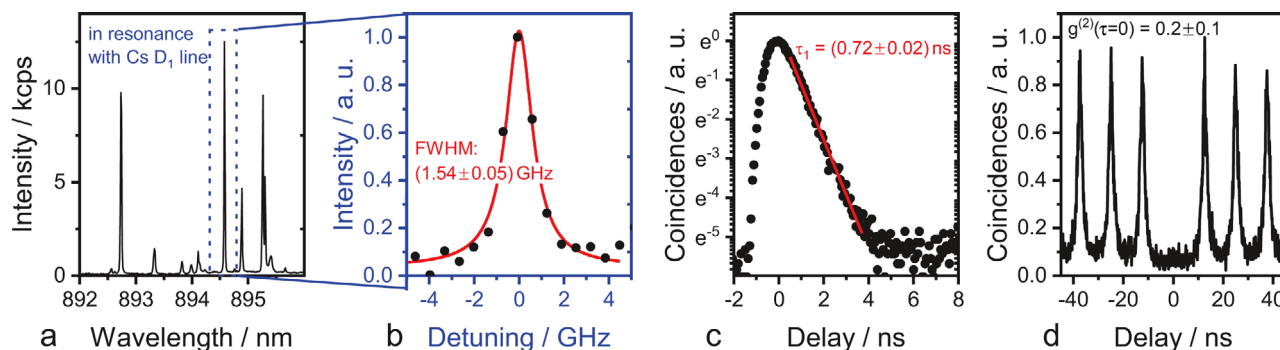
**ADVANCED
SCIENCE NEWS**

www.advancedsciencenews.com

**ADVANCED
QUANTUM
TECHNOLOGIES**

www.advquantumtech.com

Figure 5. a) µPL spectrum of the QD-microlens excited at saturation with 80 MHz repetition frequency. The marked emission line can be tuned into resonance with the Cs-D_1 line by temperature variation of the QD. b) High-resolution spectrum of the corresponding QD measured with an FPI. The red curve shows a Lorentzian fitted to the measurement data. c) Lifetime measurement for the QD emission line from (b). The lifetime $\tau_1 = (0.72 \pm 0.02)$ ns is extracted from a linear fit to the falling edge of the pulse. The coincidences are scaled logarithmically. d) Measured HBT autocorrelation function for the QD reveals high multi-photon-suppression with $g^{(2)}(0) \ll 0.5$.

experiments, an exponentially modified Gaussian function $\gamma(\tau)$ is assumed based on Wildmann's model.[18]

$$\gamma(\tau) = \frac{A}{t_0} e^{\frac{1}{2}\left(\frac{w_t}{t_0}\right)^2 - \frac{\tau - \tau_c}{t_0}} \left(\frac{1}{2} + \frac{1}{2} \mathrm{Erf} \left[\frac{\tau - \tau_c}{w_t} - \frac{w_t}{t_0} \right] \right) \quad (3)$$

A, w_t, and τ_c denote the amplitude, the standard deviation and the position of the Gaussian profile, t_0 the relaxation parameter of the exponent, and Erf(z) the Gaussian error function. The function can be obtained in its basic form from a convolution of a Gaussian function, reflecting the time resolution of the setup, and an exponential decay function, describing the decay of the excited two-level system. Using this model function, it is possible to describe both non-delayed pulses and delayed pulses subject to dispersion and to predict the expected temporal delay for different detunings and temperatures of the Cs cell. For this purpose, we describe the inhomogeneously broadened single-QD emission line by a Gaussian function. As the transmission through the Cs vapor is a function of the spectral position (see Figure 2c), the broadened QD line has to be weighted with this dependence. This dependence is considered by multiplying the two functions (in frequency representation), resulting in a modified lineshape whose frequency components are subject to individual frequency-dependent absorption. Thus, in general, the photon pulse has a non-Gaussian lineshape after passing the dispersive Cs vapor. Subsequently, the modified line shape is inserted for the amplitude A in Equation (3) and the delay for the position τ_c of the unmodified Gaussian to obtain the frequency dependent amplitude and delay of the photon pulse. The remaining parameters, $w_t = 0.54$ ns and $t_0 = 0.74$ ns are determined by fitting Equation (3) to a non-delayed pulse. Integrating the resulting expression over all relevant frequencies, a model function is obtained which phenomenologically describes the intensity of a photon pulse in the presence of absorption and dispersion as a function of time.

Taking the measured linewidth of the considered excitonic line into account, the question arises whether and at which detuning light–matter interaction with the Cs vapor can result in a complete delay of the photon pulse. In this context, we refer to complete delay, if all photons in a statistical ensemble of photon trans-

mission trials are delayed and the signal at approximately zero delay is negligible. For the given QD linewidth of 1.54 GHz, complete delay, which is highly preferable for applications, is achieved close to the Cs-D_1 line, that is, close to zero detuning, where a plateau with high transmission extends from about −2 to 3 GHz. The corresponding calculated transient is presented in **Figure 6**a for detunings in the range of −0.2 to 1.8 GHz when considering a 150 mm long Cs vapor cell at a temperature of 130 °C. In this spectral region, the entire pulse is delayed by about 14 ns, where the delayed pulse-shape depends only slightly on the detuning. In fact, a shift away from the ideal position of +840 MHz only leads to a stronger temporal broadening of the pulse but not to a splitting into a non-delayed and delayed part. The normalizations of the graphs in Figure 6a,b are chosen so that the total transmission can be read off from the respective maximum of a curve. From the inset of Figure 6a it becomes clear, that only for linewidths larger than 10 GHz a pronounced weakly delayed second pulse is formed. This comparatively wide spectral range is an advantage of Cs over Rubidium, where this window is smaller (≈7 GHz). In contrast, it is not possible to completely delay the pulse for the given linewidth in the area of strong anomalous dispersion. This is shown in Figure 6b for a vapor temperature of 70 °C. In addition to the strongly delayed part, a weakly delayed pulse is always formed, the intensity of which increases with increasing distance from the ideal position of +5067 MHz. If the ideal position is met exactly, the intensity of the components is approximately the same. Further simulations, considering the resulting pulse shape as a function of the QD linewidth, show that linewidths below 900 MHz are necessary in the region of strong anomalous dispersion to achieve a complete pulse delay (see inset of Figure 6b). Based on these theoretical considerations, in experiment, the QD emission line was shifted by temperature tuning to the optimum position of +840 MHz. Noteworthy, it is non-trivial to exactly match this target spectral position due to the technically demanding calibration in the absolute spectral position of the FPI and because sub-0.1-K temperature changes already lead to spectral shifts of 0.2 GHz, taking the measured temperature coefficient of 2.1 GHz K^{-1} in the temperature range around 12 K into account. Fits to the experimental delay data (see Figure 6c) revealed that the spectral matching of the QD line was
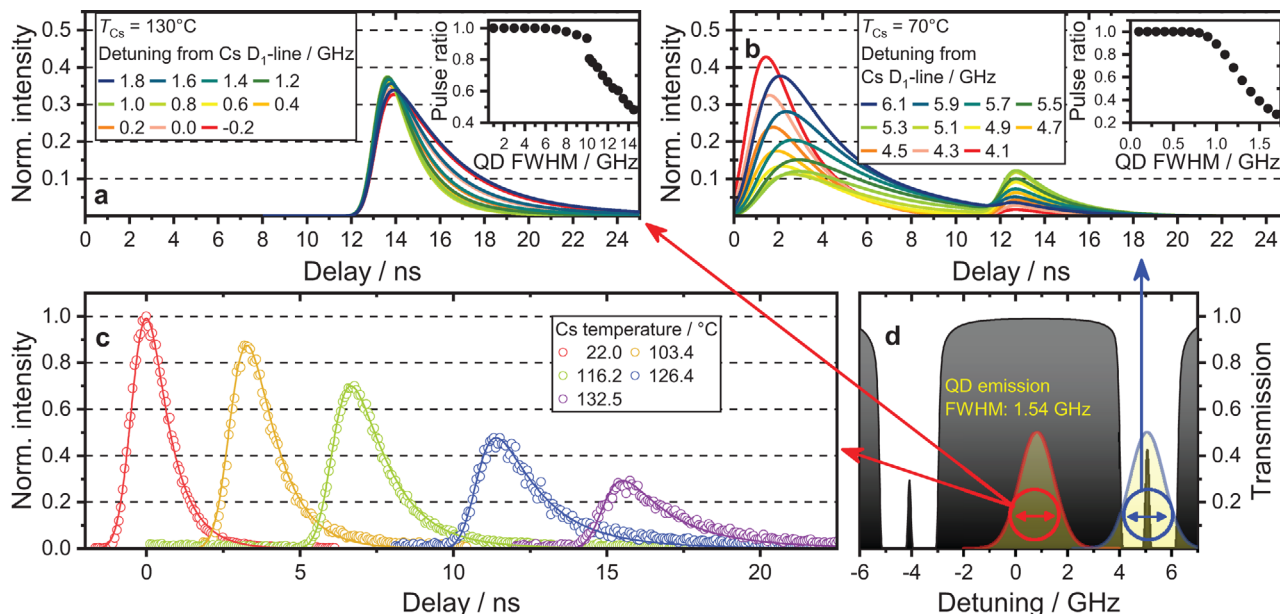
ADVANCED
SCIENCE NEWS
www.advancedsciencenews.com

ADVANCED
QUANTUM
TECHNOLOGIES
www.advquantumtech.com

Figure 6. a,b) Simulations of the photon delay in a 150 mm long Cs vapor cell. A spectral Gaussian emission line with a FWHM of 1.54 GHz is assumed for different spectral detunings relative to the Cs-D_1-line. The graphs are normalized so that the value of the global maximum of a curve corresponds to the total transmission of the pulse. The relative position of the emission line is varied and the vapor temperature (130 °C for (a) and 70 °C for (b)) is kept constant. The insets show the respective fraction of strongly delayed photons of the total integrated pulse area as a function of the linewidth (FWHM) of the QD line. The ideal position of a) +840 MHz and b) +5067 MHz was assumed. c) Experimental results (circles) obtained for single photons emitted from QD-microlenses that are delayed by a Cs vapor cell with an effective length of 150 mm. The experimental data are well described by simulations (solid lines) based on Equation (3). d) Calculated transmission versus detuning for a 150 mm long Cs vapor cell at 70 °C.

actually not perfect in our experiment (+1350 MHz instead of +840 MHz). This slight detuning of the frequency, which is more than an order of magnitude below the monochromator resolution, is not attributable to the accuracy of the temperature tuning, but to the aforementioned difficulty of precisely determining absolute frequencies. The temperature control took place with an accuracy of about 0.02 K, which corresponds to an uncertainty of the central frequency of the QD line of 42 MHz.

The measured PL transients are presented in Figure 6c, where the normalization of the curves was chosen based on the corresponding simulations. The absorption could not be measured accurately, since the count rate changed on time scales of a few minutes due to sample drifts. In addition, the setup efficiency was affected by the cells' heating power, as the nearby mirrors in the beam path were slightly misaligned at high cell temperatures.

As the vapor temperature increases, also the delay of the pulse increases as expected. All measured delays are accurately reproduced by the simulations. We achieved a complete pulse delay of (15.7 ± 0.1) ns. For a comparison with the maximum delays achieved in previous reports, the delay is considered independent of the length of the vapor cell. The measured delay achieved in our experiment of (1.05 ± 0.01) ns cm^{-1} almost reaches the highest value reported so far (1.08 ns cm^{-1}[19]), while clearly outperforming other works (0.27 ns cm^{-1},[26] 0.36 ns cm^{-1},[18] and a partial delay of 0.96 ns cm^{-1}[17]). The resulting transmission of 29%—subsequently determined by a simulation—is comparatively high due to the narrow emission linewidth of the QD-microlens. Simulations show that the transmission of a 150 mm long Cs vapor cell at a temperature of 132.5 °C is at least 15%
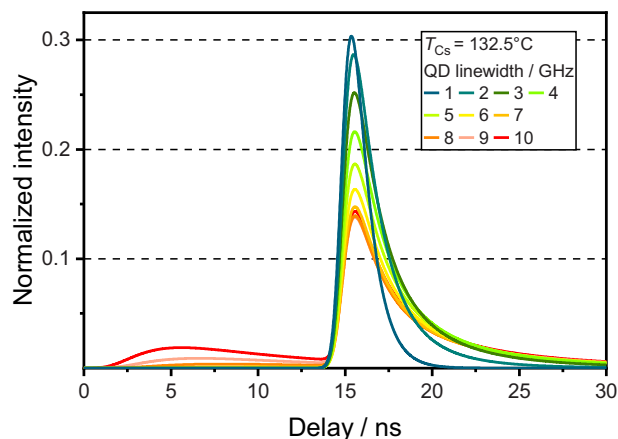

Figure 7. Simulations of the photon delay in a 150 mm long Cs vapor cell for different QD linewidths. A spectral Gaussian emission line with a FWHM of 1.54 GHz at +840 MHz with respect to the Cs-D_1-line is assumed. The graphs are normalized so that the value of the global maximum of a curve corresponds to the total transmission of the pulse.

higher compared to values reported in ref. [19] (recalculated to the same cell length) due to the significantly smaller linewidth in our experiment. Also, the group velocity dispersion (GVD) is reduced accordingly. The significant influence of the linewidth on pulse-shape and absorption can also be seen in **Figure 7**, which shows the photon delay for different line widths. On the one hand, the previously described occurrence of an undelayed

**ADVANCED
SCIENCE NEWS**

www.advancedsciencenews.com

**ADVANCED
QUANTUM
TECHNOLOGIES**

www.advquantumtech.com

fraction for large linewidths can be observed. On the other hand, the influence of the linewidth in the sub-GHz range manifests itself in the decreasing transmission with increasing linewidth and, in addition, the GVD depends strongly on the spectral width. This results in a strong disturbance of the temporal pulse-shape for linewidths >2 GHz.

4. Conclusion

In the present work, we explored light–matter coupling in a Cs vapor cell, which allowed us to delay single photons emitted from a deterministically fabricated QD-microlens. The latter were realized by a 3D in situ EBL process by selecting bright QDs with suitable emission wavelength and integrating them in monolithic QD-microlenses via a plasma etching step. This way, we enhance the photon extraction efficiency of target QDs emitting at Cs-D_1 line compatible wavelength. The excellent optical properties of the fabricated SPSs are reflected in a narrow QD linewidth of 1.54 GHz, being crucial for the interfacing of QD lines with atomic vapor, as absorption and GVD are determined by this important property. Using detailed numerical simulations, the influence of the spectral position and the linewidth of the QD emission on the resulting temporal shape of a light pulse after passing through the Cs vapor was investigated for different vapor temperatures in the range of 25 to 140 °C. It was shown that the local maximum in the transmission of Cs vapor at +840 MHz relative to the Cs-D_1 line is superior to that at −4085 and +5067 MHz, not only due to the broader spectral window, but also due to the lower absorption for a given temporal delay. Based on the simulations, it was possible to delay photons emitted by a QD-microlens at a maximum of (15.71 ± 0.01) ns (corresponding to (1.05 ± 0.01) ns cm^{-1}) under optimized experimental conditions. Moreover, due to the narrow linewidth of the studied QD-exciton of 1.54 GHz, the light pulse was completely delayed with comparatively low absorption and a low distortion of the original pulse shape due to the small group velocity dispersion. Our results highlight the high potential of light–matter interaction in dilute Cs vapor to control the propagation of single photons emitted by deterministically fabricated quantum light sources. In future, such precisely engineered quantum light emitters could enable the realization of flexible photon delay modules and quantum memories with a variety of applications in photonic quantum technology.

Conflict of Interest

The authors declare no conflict of interest.

[1] L.-M. Duan, M. D. Lukin, J. I. Cirac, P. Zoller, *Nature* **2001**, *414*, 413.

[2] N. Sangouard, C. Simon, H. de Riedmatten, N. Gisin, *Rev. Mod. Phys.* **2011**, *83*, 33.

[3] a) K. S. Choi, H. Deng, J. Laurat, H. J. Kimble, *Nature* **2008**, *452*, 67; b) F. Bussières, N. Sangouard, M. Afzelius, H. de Riedmatten, C. Simon, W. Tittel, *J. Mod. Optic.* **2013**, *60*, 1519.

[4] J. Wolters, G. Buser, A. Horsley, L. Béguin, A. Jöckel, J.-P. Jahn, R. J. Warburton, P. Treutlein, *Phys. Rev. Lett.* **2017**, *119*, 060502.

[5] a) N. Akopian, R. Trotta, E. Zallo, S. Kumar, P. Atkinson, A. Rastelli, O. G. Schmidt, V. Zwiller, *arXiv:1302.2005*, **2013**; b) L. Leandro, C. P. Gunnarsson, R. Reznik, K. D. Jöns, I. Shtrom, A. Khrebtov, T. Kasama, V. Zwiller, G. Cirlin, N. Akopian, *Nano Lett.* **2018**, *18*, 7217; c) M. Zopf, T. Macha, R. Keil, E. Uruñuela, Y. Chen, W. Alt, L. Ratschbacher, F. Ding, D. Meschede, O. G. Schmidt, *Phys. Rev. B* **2018**, *98*, 161302.

[6] A. Acín, I. Bloch, H. Buhrman, T. Calarco, C. Eichler, J. Eisert, D. Esteve, N. Gisin, S. J. Glaser, F. Jelezko, S. Kuhr, M. Lewenstein, M. F. Riedel, P. O Schmidt, R. Thew, A. Wallraff, I. Walmsley, F. K. Wilhelm, *New J. Phys.* **2018**, *20*, 080201.

[7] a) H.-J. Briegel, W. Dür, J. I. Cirac, P. Zoller, *Phys. Rev. Lett.* **1998**, *81*, 5932; b) N. Gisin, R. Thew, *Nat. Photonics* **2007**, *1*, 165.

[8] N. Sangouard, C. Simon, J. Minář, H. Zbinden, H. de Riedmatten, N. Gisin, *Phys. Rev. A* **2007**, *76*, 050301.

[9] a) J.-W. Pan, Z.-B. Chen, C.-Y. Lu, H. Weinfurter, A. Zeilinger, M. Żukowski, *Rev. Mod. Phys.* **2012**, *84*, 777; b) F. B. Basset, M. B. Rota, C. Schimpf, D. Tedeschi, K. D. Zeuner, S. F. Covre da Silva, M. Reindl, V. Zwiller, K. D. Jöns, A. Rastelli, R. Trotta, *arXiv:1901.06646*, **2019**.

[10] a) G. Alzetta, A. Gozzini, L. Moi, G. Orriols, *Il Nuovo Cimento B 11 1976*, *36*, 5; b) E. Arimondo, G. Orriols, *Lettere Al Nuovo Cimento 2 1976*, *17*, 333; c) S. E. Harris, *Phys. Today* **1997**, *50*, 36.

[11] a) P. Michler, A. Kiraz, C. Becher, W. V. Schoenfeld, P. M. Petroff, L. Zhang, E. Hu, A. Imamoğlu, *Science* **2000**, *290*, 2282; b) C. Santori, D. Fattal, J. Vučković, G. S. Solomon, Y. Yamamoto, *Nature* **2002**, *419*, 594; c) H. Wang, H. Hu, T.-H. Chung, J. Qin, X. Yang, J.-P. Li, R.-Z. Liu, H.-S. Zhong, Y.-M. He, X. Ding, Y.-H. Deng, Q. Dai, Y.-H. Huo, S. Höfling, C.-Y. Lu, J.-W. Pan, *Phys. Rev. Lett.* **2019**, *122*, 113602; d) J. Liu, R. Su, Y. Wei, B. Yao, S. F. Covre da Silva, Y. Yu, J. Iles-Smith, K. Srinivasan, A. Rastelli, J. Li, X. Wang, *Nat. Nanotechnol.* **2019**, *14*, 586.

[12] M. Gschrey, A. Thoma, P. Schnauber, M. Seifried, R. Schmidt, B. Wohlfeil, L. Krüger, J.-H. Schulze, T. Heindel, S. Burger, F. Schmidt, A. Strittmatter, S. Rodt, S. Reitzenstein, *Nat. Commun.* **2015**, *6*, 7662.

[13] N. Somaschi, V. Giesz, L. de Santis, J. C. Loredo, M. P. Almeida, G. Hornecker, S. L. Portalupi, T. Grange, C. Antón, J. Demory, C. Gómez, I. Sagnes, N. D. Lanzillotti-Kimura, A. Lemaître, A. Auffeves, A. G. White, L. Lanco, P. Senellart, *Nat. Photonics* **2016**, *10*, 340.

[14] S. Unsleber, Y.-M. He, S. Gerhardt, S. Maier, C.-Y. Lu, J.-W. Pan, N. Gregersen, M. Kamp, C. Schneider, S. Höfling, *Opt. Express* **2016**, *24*, 8539.

[15] B. Wu, J. F. Hulbert, E. J. Lunt, K. Hurd, A. R. Hawkins, H. Schmidt, *Nat. Photonics* **2010**, *4*, 776.

[16] L. Schweickert, K. D. Jöns, M. Namazi, G. Cui, T. Lettner, K. D. Zeuner, L. S. Montaña, S. F. Covre da Silva, M. Reindl, H. Huang, R. Trotta, A. Rastelli, V. Zwiller, E. Figueroa, *arXiv:1808.05921*, **2018**.

[17] N. Akopian, L. Wang, A. Rastelli, O. G. Schmidt, V. Zwiller, *Nat. Photonics* **2011**, *5*, 230.

[18] J. S. Wildmann, R. Trotta, J. Martín-Sánchez, E. Zallo, M. O'Steen, O. G. Schmidt, A. Rastelli, *Phys. Rev. B* **2015**, *92*, 235306.

[19] H. Vural, S. L. Portalupi, J. Maisch, S. Kern, J. H. Weber, M. Jetter, J. Wrachtrup, R. Löw, I. Gerhardt, P. Michler, *Optica* **2018**, *5*, 367.

[20] A. Schlehahn, R. Schmidt, C. Hopfmann, J.-H. Schulze, A. Strittmatter, T. Heindel, L. Gantz, E. R. Schmidgall, D. Gershoni, S. Reitzenstein, *Appl. Phys. Lett.* **2016**, *108*, 021104.

[21] M. Gschrey, F. Gericke, A. Schüßler, R. Schmidt, J.-H. Schulze, T. Heindel, S. Rodt, A. Strittmatter, S. Reitzenstein, *Appl. Phys. Lett.* **2013**, *102*, 251113.

[22] T. Udem, J. Reichert, R. Holzwarth, T. W. Hänsch, *Phys. Rev. Lett.* **1999**, *82*, 3568.

[23] M. Gschrey, R. Schmidt, J.-H. Schulze, A. Strittmatter, S. Rodt, S. Reitzenstein, *J. Vac. Sci. Technol., B: Nanotechnol. Microelectron.: Mater., Process., Meas., Phenom.* **2015**, *33*, 021603.

[24] M. A. Zentile, J. Keaveney, L. Weller, D. J. Whiting, C. S. Adams, I. G. Hughes, *Comput. Phys. Commun.* **2015**, *189*, 162.

[25] W. Demtröder, in *Laserspektroskopie: Grundlagen und Techniken*, Edition 5, Springer, Berlin **2007**, p. 453.

[26] R. Trotta, J. Martín-Sánchez, J. S. Wildmann, G. Piredda, M. Reindl, C. Schimpf, E. Zallo, S. Stroj, J. Edlinger, A. Rastelli, *Nat. Commun.* **2016**, *7*, 10375.

1900071 (8 of 8)